Document Version:
Publisher's PDF, also known as Version of record

Queen's University Belfast - Research Portal:
Link to publication record in Queen's University Belfast Research Portal

P H Y S I C A L   R E V I E W   L E T T E R S

Coexistence of Weak Ferromagnetism and Ferroelectricity in the High Pressure $LiNbO_3$-Type Phase of $FeTiO_3$

T. Varga,[1,][*] A. Kumar,[2] E. Vlahos,[2] S. Denev,[2] M. Park,[3] S. Hong,[1] T. Sanehira,[4] Y. Wang,[4] C. J. Fennie,[5] S. K. Streiffer,[6] X. Ke,[7] P. Schiffer,[7] V. Gopalan,[2] and J. F. Mitchell[1]

[1]*Materials Science Division, Argonne National Laboratory, Argonne Illinois 60439, USA*
[2]*Department of Materials Science and Engineering, Pennsylvania State University, University Park, Pennsylvania 16802, USA*
[3]*Department of Materials Science and Engineering, Korea Advanced Institute of Science and Technology, Daejon 305-701, Korea*
[4]*Center for Advanced Radiation Sources, The University of Chicago, Chicago, Illinois 60637, USA*
[5]*Department of Applied and Engineering Physics, Cornell University, Ithaca, New York 14853, USA*
[6]*Center for Nanoscale Materials, Argonne National Laboratory, Argonne, Illinois 60439, USA*
[7]*Department of Physics and Materials Research Institute, Pennsylvania State University, University Park, Pennsylvania 16802, USA*
(Received 10 March 2009; published 24 July 2009)

We report the magnetic and electrical characteristics of polycrystalline $FeTiO_3$ synthesized at high pressure that is isostructural with acentric $LiNbO_3$ (LBO). Piezoresponse force microscopy, optical second harmonic generation, and magnetometry demonstrate ferroelectricity at and below room temperature and weak ferromagnetism below ~ 120 K. These results validate symmetry-based criteria and first-principles calculations of the coexistence of ferroelectricity and weak ferromagnetism in a series of transition metal titanates crystallizing in the LBO structure.

Multiferroics are materials in which seemingly contraindicated ferroic properties, e.g., magnetism and polar order, coexist [1,2]. Magnetic ferroelectrics for which the different ferroic orders couple, either macroscopically through interfacial magnetostriction [3,4] or microscopically via exchange striction [5], may be promising materials for applications in memories, sensors, actuators, and other multifunctional devices. They also offer a rich opportunity to study fundamental aspects of spin-lattice coupling. In the case of bulk materials, several neutron diffraction studies point to a spiral magnetic state as an essential ingredient for coupling between magnetism and ferroelectricity [5–7]. Phenomenological [8] as well as first principles explanations [9] of the connection between ferroelectricity and the magnetic spiral link polar and magnetic orders through the product $\mathbf{P} \sim \mathbf{e} \times \mathbf{Q}$, where $\mathbf{e}$ is a unit vector along the spin rotation axis and $\mathbf{Q}$ is the spiral propagation vector. The microscopic origin of this form can be traced to the antisymmetric Dzyaloshinskii-Moriya (D-M) interaction [1], which can lead to inhomogeneous states, such as the magnetic spiral found in $BiFeO_3$. Because of the nature of the magnetic spiral, no net ferromagnetic moment is found in such systems.

The D-M interaction can alternatively lead to weak ferromagnetism (WFM), as observed in manganites [10] and other transition metal oxides, such as rare-earth orthoferrites [11,12]. WFM in a material that is simultaneously ferroelectric is particularly interesting as it has been recently discussed as the best route to achieve electric field control of 180° switching of ferromagnetic domains [13,14], yet identifying a material with the required coupling, even in principle, has proven challenging. Recently, Fennie has argued from symmetry principles that polar or-

der will induce a nonzero staggered D-M interaction, and hence weak ferromagnetism, when an invariant of the form $E \sim \mathbf{P} \cdot (\mathbf{L} \times \mathbf{M})$—where $\mathbf{P}$, $\mathbf{L}$, and $\mathbf{M}$ are polar, antiferromagnetic and magnetization vectors, respectively—exists in the phenomenological free energy functional of the putative high temperature antiferromagnetic, paraelectric parent. Fennie argued that materials crystallizing in the high pressure form, i.e., the $LiNbO_3$ phase, of $FeTiO_3$, $MnTiO_3$, and $NiTiO_3$, are candidate materials that exhibit the required coupling [14]. Additionally, first-principles calculations on these materials indicate that they would have extremely high polarization, comparable to that of $BiFeO_3$ [2], making them attractive targets in the search for new multiferroic systems.

In this Letter we report the synthesis and characterization of the high pressure form of $FeTiO_3$ ($FeTiO_3$-II), which is found to be ferroelectric at and below room temperature and weakly ferromagnetic below ~ 120 K. These results validate Fennie's predicted coexistence of weak ferromagnetism and ferroelectric polarization in this class of materials [14]. From a fundamental standpoint, this is particularly important, as $FeTiO_3$-II stands as an extremely rare example of a ferroelectric exhibiting WFM arising from the D-M interaction. Our results furthermore provide a significant step toward establishing $FeTiO_3$-II as a prototype bulk multiferroic whose magnetic structure can in principle be switched by reversing an applied electric field.

Following the discussion of [15], we prepared $FeTiO_3$-II from ilmenite at 18 GPa and 1200 °C using a multianvil press at the 13-ID-D beam line (GSECARS) of the Advanced Photon Source (APS). Topographic imaging of the product by atomic force microcopy reveals a typical

grain size of about 400 nm [see Fig. 1(a)], and energy-dispersive spectroscopy (EDS) analysis of several grains confirms the Fe:Ti stoichiometry. Synchrotron powder x-ray diffraction (SXRD) data were collected at 298 K on the 11-BM-B beam line at the APS. The SXRD data were refined with the Rietveld method using the published crystal structure of $FeTiO_3$-II [16] as a starting point. Details can be found in the supplementary material [17].

We have explored the polar properties of $FeTiO_3$-II using piezoresponse force microscopy (PFM) and optical second harmonic generation (SHG): both techniques indicate that $FeTiO_3$-II is ferroelectric at room temperature. We note that dielectric tangent losses of ~ 1.18 (1 MHz) at room temperature prevented direct electrical polarization hysteresis measurements. At 100 K, the losses reduce to ~ 0.027 at 1 MHz, but saturated loops could not be obtained indicating that the coercive field exceeds the ± 15 kV/cm we were able to apply.

Out-of-plane PFM imaging has been used to confirm the detailed ferroelectric domain configuration at the nanoscale [18,19]. The amplitude images in Fig. 1(b) show the varying degrees of alignment of polarization vectors to the surface normal in each domain, and reveal the various distributions of polarization vectors. The phase images [Fig. 1(c)] sample the direction of polarization vectors showing the expected mixture of up (dark contrast) and down (bright contrast) polar domains.

A stationary-tip piezoresponse hysteresis loop obtained by applying $0.5V_{rms}$ to the tip while sweeping the dc voltage from -10 V to 10 V to the bottom electrode with frequency of 41.7 mHz is shown in Fig. 1(d). Although strong imprint of the loop, which could be due to the strong bias field created by unswitched polarization beneath the grain of interest, is apparent along both the electric field and piezoelectric coefficient axes, this measurement is sufficient to demonstrate a reversible polar response and therefore ferroelectricity. It is important to note that spatial variation of electromechanical properties was observed. This indicates that these samples are not fully homogeneous, which is not unexpected for this stage of synthesis development.

Ferroelectricity is further established in $FeTiO_3$-II via optical second harmonic generation (SHG), which involves the conversion of light at a frequency ω (electric field E^ω) into an optical signal at a frequency 2ω by a nonlinear medium through the creation of a nonlinear polarization $P_i^{2\omega} = d_{ijk}E_j^\omega E_k^\omega$, where d_{ijk} represents the nonlinear optical tensor coefficients (not to be confused with the piezoelectric tensor). Optical SHG mapping was performed with a fundamental wave generated from a tunable Ti-sapphire laser with 65-fs pulses of wavelength 800 nm incident normal to the sample surface. Two-dimensional mapping of the signal was done using a WITec Alpha 300 S confocal microscope.

While the stabilized $LiNbO_3$ phase of $FeTiO_3$ shows a strong SHG contrast [Fig. 2(a)], no signal was observable
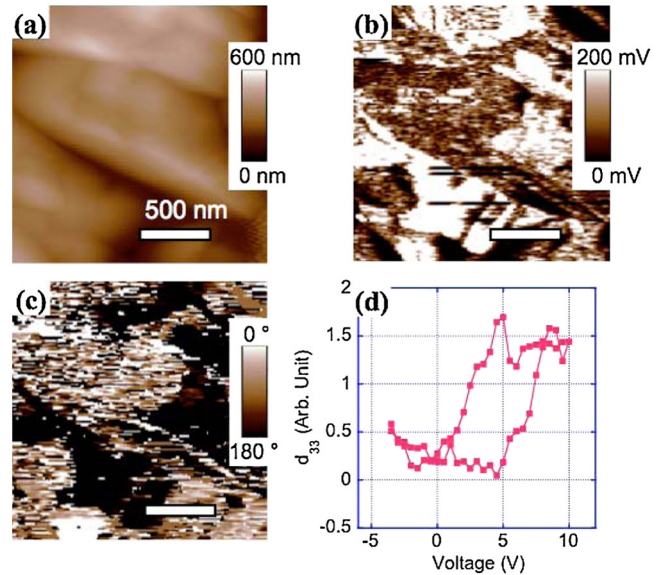

FIG. 1 (color online). Surface topography (a), out-of-plane PFM amplitude (b) and phase (c) images in $FeTiO_3$ bulk crystal sample. Bright contrasts in amplitude correspond to polarization vectors strongly aligned to the surface normal (either positive or negative normal direction). (d) Local piezoresponse hysteresis loops were collected inside a grain.

in the ilmenite phase [Fig. 2(b)]. These results confirm that the high-pressure phase is polar while the ilmenite phase is nonpolar. The spatial variation of the SHG signal in Fig. 2(a) can arise from differently oriented polycrystallites as well as multidomain structure. The SHG hysteresis loops at different spots on the sample were measured using electrodes applied on opposite edges of the sample while probing the top surface. A representative measurement is shown in Fig. 2(c), and has the "butterfly" shape characteristic of the response of a ferroelectric. We reasonably exclude effects such as electric-field induced SHG (EFISH) as insignificant, since no such effects are seen in the compositionally similar Ilmenite phase under an electric field. The corresponding polarization hysteresis loop shown in Fig. 2(c) can be derived from the SHG intensity vs electric-field data as follows: the SHG $I^{2\omega} \propto d_{ijk}^2 \propto (\chi_{ijks}P_s)^2$, where χ_{ijks} represents the fourth order nonlinear optical susceptibility tensor in the paraelectric phase. Though points 1 and 3 in Fig. 2(c) of the butterfly loop correspond to the field axis crossings of the polarization hysteresis loops, the SHG intensity is not exactly zero at these minima, due to an incomplete cross cancellation of the SHG intensity between antiparallel domains in the area of the sample being probed. Thus, in going from the SHG intensity to the switchable polarization loops, we first subtract a baseline intensity corresponding to a linear extrapolation between two minima (1 and 3), followed by taking the square root of the intensity, and finally switching the sign of the result only for the segment of the butterfly loop 1-2-3 in Fig. 2(c). This yields a polarization hysteresis loop that is proportional to the net *switchable* polarization
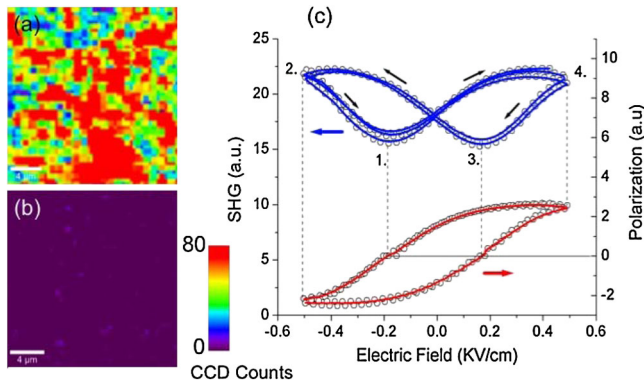
FIG. 2 (color online). SHG mapping of polar regions at 296 K in (a) stabilized high pressure phase of $FeTiO_3$ with $LiNbO_3$ crystal structure (noncentrosymmetric), (b) pure ilmenite phase (centrosymmetric). (c) SHG "butterfly" hysteresis loops (blue) at a fixed point in (a) with applied electric fields at 296 K and the corresponding polarization hysteresis loop (red) (see text). The polarization of fundamental light was horizontal, and all the output SHG polarizations were detected without an exit analyzer.

within the probe region, and clearly confirms the presence of ferroelectricity at room temperature. Additionally, the SHG intensity was observed down to 5 K, indicating that the $FeTiO_3$-II is polar in the low temperature regime. Thus switchability has been clearly established, the critical proof for ferroelectricity given the polar crystal structure. The magnitude of saturated polarization remains to be determined.

The dc SQUID magnetization data measured in 1 kOe (see supplementary material [17]) yield a linear χ^{-1} vs T for $150\ K < T < 250\ K$. The extracted $p_{eff} = 5.6\mu_B/Fe$ is consistent with that reported for ambient-pressure ilmenite ($p_{eff} = 5.62\mu_B/Fe$ [20]). A measured $\theta_W = -248\ K$ agrees well with the first-principles predicted value of $-305\ K$ [21]. We note that θ_W and T_N for ilmenite are 23 K and 55 K, respectively [22], demonstrating a substantially modified magnetic exchange among Fe^{2+} ions in the high pressure phase.

Figure 3(a) compares the ac magnetic susceptibility of an ilmenite sample to that of $FeTiO_3$-II. The antiferromagnetic transition of ilmenite at ~55 K is replaced by a sharp cusp at $T \sim 110$ K. We also find a clear anomaly in the heat capacity [Fig. 3(b)] near this temperature. This thermodynamic signature—combined with a lack of frequency dependence in the 1–10 kHz range—demonstrate that below 110 K $FeTiO_3$-II is a long-range ordered antiferromagnet, in agreement with the theoretical prediction [14]. Figure 3(c) shows isothermal magnetization measured at 105 K, just below T_N. A clear hysteresis is observed in the data, indicative of a WFM component superimposed on the antiferromagnetic background. We note that $M(H)$ measured above 120 K shows no hysteresis [Fig. 3(c), top left inset], demonstrating that the appearance of WFM is linked to the onset of the antiferromagnetic (AFM) state. A small curvature observed below ~1 kOe [Fig. 3(c), top left inset] is seen in the range $5\ K \leq T \leq 300\ K$ and may reflect an
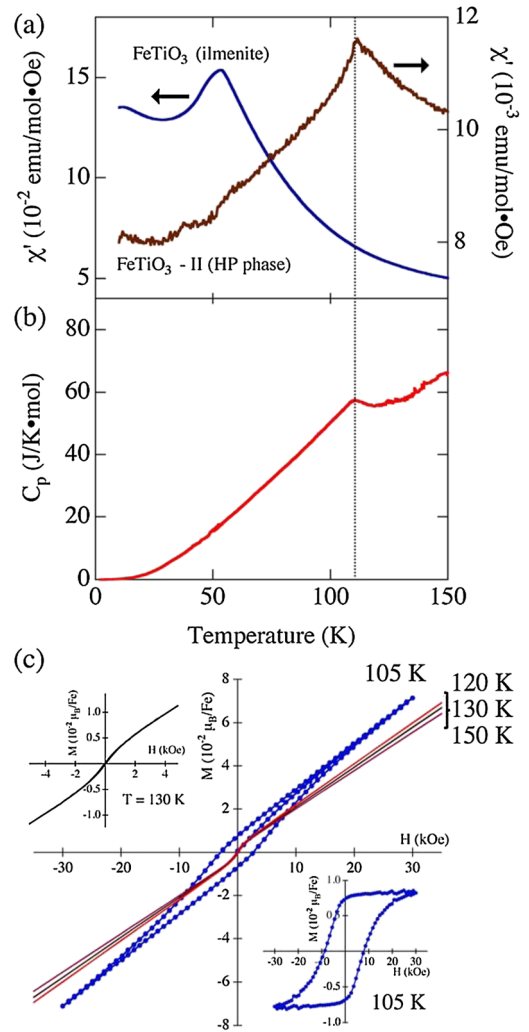

FIG. 3 (color online). (a) Magnetic susceptibility of $FeTiO_3$ (ilmenite) and high-pressure $FeTiO_3$-II. (b) Specific heat of high-pressure $FeTiO_3$-II. (c) Isothermal magnetization of $FeTiO_3$-II following zero-field cooling. See text for details.

extremely low concentration of a magnetic impurity such as Fe (found at ~1% level by XRD) or ferrous oxides in quantities undetectable to XRD. In the bottom right inset of Fig. 3(c) we have subtracted the high field linear part of $M(H)$ to estimate the field dependence of the ferromagnetic (FM) component alone. This analysis shows a symmetric hysteresis loop, saturating by 30 kOe at $0.008\mu_B/Fe$. There are two possible origins for the intrinsic WFM: (1) phase separation into discrete FM and AFM regions in the sample, as has been proposed both theoretically [23] and experimentally [24] for several doped transition metal oxides, or (2) a canting of the Fe spins away from 180°. The former scenario is unlikely based on the coincident appearance of both FM and AFM components and the lack of frequency dependence in the ac susceptibility, leading us to favor the canted state as the origin of WFM.

Several facts argue that the weak ferromagnetic signal is intrinsic to the $FeTiO_3$-II phase (see supplementary mate-

rial [17]): (1) None of the iron-containing impurity phases (all in $\sim 1\%$ level) found in the Rietveld analysis of the x-ray data have ferromagnetic transition temperatures near 110 K. (2) The specific heat [Fig. 3(b)] shows a well-defined anomaly centered at 110 K with amplitude exceeding what could be accounted for by a $\sim 1\%$ ferromagnetic impurity such as Fe_3O_4 (with its Verwey transition at ~ 120 K), and an impurity ferromagnetic phase large enough to account for our heat capacity signal would yield orders of magnitude larger magnetic signal. (3) Measurement of a second sample prepared under different conditions yields both qualitatively and quantitatively consistent magnetic behavior.

We can estimate the canting angle of the WFM by invoking the symmetry arguments of Ref. [14] under the assumption that the polar domains are randomly and uniformly distributed in the polycrystalline sample [25]. According to Ref. [14] the magnetization vector, **M**, of each magnetic domain within a given polar domain will lie perpendicular to the polar vector **P**. However, in $\mathbf{H} = 0$ (or ignoring higher order single-ion anisotropy), this coupling does not fully constrain the various magnetic domains within each polar domain, as each magnetic domain need only satisfy $\mathbf{P} \cdot \mathbf{M} = 0$ individually. Application of a sufficiently large magnetic field will rotate **M** about **P** to maximize $\mathbf{M} \cdot \mathbf{H}$ subject to this constraint, orienting **P**, **H**, and **M** coplanar within that polar domain. In this case, the projection of **M** onto **H** is $M_H = M \sin\theta$, where θ is the polar angle between **P** and **H**. Averaging over θ, accounting for $T/T_C \sim 0.9$ and using the extracted estimate of $M_H = 0.008\mu_B/$Fe yields $M_S = 0.04\mu_B/$Fe, in excellent agreement with the value $0.03\mu_B/$Fe calculated in Ref. [14].

In summary, we have prepared the $LiNbO_3$ polymorph of ilmenite, $FeTiO_3$-II, at high pressure and found that it is both ferroelectric and weakly ferromagnetic, in agreement with the first-principles calculations of [14]. Although not offering definitive proof that the polarization is causal for the WFM, our results validate this rare weak-ferromagnetic and ferroelectric state predicted in Ref. [14], which offers a strong symmetry argument and direct first-principles calculations that this spin canting can only arise due to the presence of the polar lattice distortion. For definitive proof of this effect, it remains to demonstrate explicitly using aligned single crystals that the magnetic and polar domains can be switched in concert.

*Present address: Environmental and Molecular Sciences Laboratory, Pacific Northwest National Laboratory, Richland, Washington 99352, USA .

[1] S.-W. Cheong and M. Mostovoy, Nature Mater. **6**, 13 (2007).
[2] R. Ramesh and N. A. Spaldin, Nature Mater. **6**, 21 (2007).
[3] G. Srinivasan, E. T. Rasmussen, and B. J. Levin *et al.*, Phys. Rev. B **65**, 134402 (2002).
[4] G. Srinivasan, E. T. Rasmussen, and B. J. Levin *et al.*, Phys. Rev. B **66**, 029901 (2002).
[5] M. Kenzelmann, A. B. Harris, and S. Jonas *et al.*, Phys. Rev. Lett. **95**, 087206 (2005).
[6] O. Prokhnenko, R. Feyerherm, and E. Dudzik *et al.*, Phys. Rev. Lett. **98**, 057206 (2007).
[7] O. P. Vajk, M. Kenzelmann, and J. W. Lynn *et al.*, J. Appl. Phys. **99**, 08E301 (2006).
[8] M. Mostovoy, Phys. Rev. Lett. **96**, 067601 (2006).
[9] H. Katsura, N. Nagaosa, and A. V. Balatsky, Phys. Rev. Lett. **95**, 057205 (2005).
[10] V. Skumryev *et al.*, Eur. Phys. J. B **11**, 401 (1999).
[11] G. W. Durbin, C. E. Johnson, and M. F. Thomas, J. Phys. C **10**, 1975 (1977).
[12] R. L. White, J. Appl. Phys. **40**, 1061 (1969).
[13] C. Ederer and N. A. Spaldin, Phys. Rev. B **71**, 060401 (2005).
[14] C. J. Fennie, Phys. Rev. Lett. **100**, 167203 (2008).
[15] A. Mehta *et al.*, Phys. Chem. Miner. **21**, 207 (1994).
[16] K. Leinenweber *et al.*, Phys. Chem. Miner. **22**, 251 (1995).
[17] See EPAPS Document No. E-PRLTAO-103-046931 for supplementary data including dc susceptibility, heat capacity, additional magnetic and piezoforce microscopy data as well as detailed crystallographic refinements. For more information on EPAPS, see http://www.aip.org/pubservs/epaps.html.
[18] S. Hong *et al.*, J. Appl. Phys. **105**, 061619 (2009).
[19] S. Hong *et al.*, Appl. Phys. Lett. **84**, 2382 (2004).
[20] Y. Ishikawa and S.-i. Akimoto, J. Phys. Soc. Jpn. **13**, 1298 (1958).
[21] C. J. Fennie, arXiv:0711.1331v2.
[22] Y. Ishikawa and S.-i. Akimoto, J. Phys. Soc. Jpn. **12**, 1083 (1957).
[23] E. Dagotto and A. Moreo, J. Magn. Magn. Mater. **226-230**, 763 (2001).
[24] I. O. Troyanchuk *et al.*, J. Phys. Condens. Matter **15**, 8865 (2003).
[25] While large magnetic fields could in principle rotate the polar domains due to the coupling of **P** to **M**, it is likely that the spin-flop field of the antiferromagnet would be reached first.